

Measurement of spin observables in the $^{28}\text{Si}(\vec{p}, \vec{p}')$ reaction at 500 MeV and comparison with the distorted-wave impulse approximation

E. Donoghue,⁽¹⁾ C. Glashauser,⁽¹⁾ N. Hintz,⁽²⁾ A. Sethi,⁽²⁾ J. Shepard,⁽³⁾ R. Fergerson,^{(1),*}
M. Franey,⁽²⁾ M. Gazzaly,⁽²⁾ K. Jones,⁽⁴⁾ J. McClelland,⁽⁴⁾ S. Nanda,^{(1),†} and M. Plum⁽⁴⁾

⁽¹⁾*Serin Physics Laboratory, Rutgers University, Piscataway, New Jersey 08854*

⁽²⁾*School of Physics and Astronomy, University of Minnesota, Minneapolis, Minnesota 55455*

⁽³⁾*Department of Physics, University of Colorado, Boulder, Colorado 80309*

⁽⁴⁾*Los Alamos Meson Physics Facility, Los Alamos National Laboratory, Los Alamos, New Mexico 87545*

(Received 21 September 1990)

Analyzing power A_y and spin-transfer observables D_{ij} have been measured for 500-MeV proton inelastic scattering from ^{28}Si . Measured values of the D_{ij} for the 9.70-MeV 5^- , $T=0$, the 11.58-MeV 6^- , $T=0$, and the 14.35-MeV 6^- , $T=1$ states are reported at 17° and 22° ; values of A_y cover the range from about 10° to 26° . Nonrelativistic (NRIA) and relativistic (RIA) impulse-approximation calculations are compared with the data. The differences between the two types of calculations are generally small. The RIA yields excellent agreement with the D_{ij} data for the 5^- state, and both RIA and NRIA do well for D_{ij} data for the 6^- , $T=0$ state but poorly for the 6^- , $T=1$ state. For the A_y data, both types of calculation give fairly good predictions for the 5^- and 6^- , $T=1$ states, but not for the 6^- , $T=0$ state. Comparison between theory and experiment for the combinations of observables D_K , which are sensitive to individual terms in the nucleon-nucleon interaction, indicates a possible need for medium corrections in the $T=1$ tensor and spin-orbit forces.

I. INTRODUCTION

Measurements of spin observables in intermediate-energy proton scattering have been rich sources of information on nuclear structure and reaction mechanisms in recent years. Interest in applications of the Dirac equation to nuclear problems has grown enormously after its success in describing analyzing powers (A_y) and spin-transfer parameters (D_{ij}) for elastic scattering.¹ Spin-transfer strength in isolated states at low excitation energies and in the continuum at high excitation energies has been identified by spin-flip probability measurements.² Complete data on the spin-transfer parameters for normal (\hat{N}), longitudinal (\hat{L}), and sideways (\hat{S}) polarized beams have permitted the separation of the spin-longitudinal and spin-transverse components of continuum excitations.³

Blezynski *et al.*⁴ and Moss⁵ have shown that complete measurements of the D_{ij} for isolated states yield information on individual components of the nucleon-nucleon (NN) force inside nuclei. The first such inelastic measurements were performed by Aas *et al.* for ^{40}Ca at 500 MeV; only natural parity states were observed and the symmetry rules for elastic scattering were followed.⁶ McClelland *et al.*⁷ took such data at 500 MeV for unnatural parity (1^+) states in ^{12}C at low momentum transfer q . A nonrelativistic distorted-wave impulse-approximation (NRIA) treatment of the reaction with the Love-Franey t matrix⁸ and Cohen-Kurath wave functions gave good agreement with the data. However, it is known that the NRIA gives a poor fit to the elastic A_y and spin-rotation parameter (Q) data. It is just here that the Dirac relativistic impulse approximation (RIA) has

been so successful.¹ A main purpose of this work is to compare relativistic and nonrelativistic impulse-approximation predictions for some *inelastic* spin observables for $^{28}\text{Si}(p, p')$ at 500 MeV at high q . The only other high q analyses available are preliminary results reported by Olmer for 200-MeV measurements⁹ on the $T=0$ and $T=1$ 4^- stretched states in ^{16}O . Some problems were found in the predictions of both relativistic and nonrelativistic calculations with several standard NN interactions which fit free scattering. It is not clear whether these problems are related to uncertainties in the nuclear structure or to changes in the NN amplitudes in the nuclear medium. A second focus of this work is the consideration of just this question—whether free NN amplitudes are capable of accounting for the D_{ij} data when the nuclear structure is simple.

Here we report data for the 5^- collective state at 9.70 MeV and the 6^- , $T=0$ (11.58 MeV) and 6^- , $T=1$ (14.35 MeV) stretched states of ^{28}Si . The 5^- state is excited by the spin-independent central (71%) and the spin-orbit (29%) components of the NN interaction. These percentages are suggested from analysis¹⁰ of differential cross-section data (σ) with the Love-Franey t matrix. The same analysis suggests that the 6^- , $T=0$ state is excited primarily by the spin-orbit force (77%) and the 6^- , $T=1$ state by the tensor force (84%). When simple ($d_{5/2}^{-1}f_{7/2}$) configurations are assumed for these stretched states, spectroscopic factors much lower than unity are seen for both states with a wide variety of probes. The strength of the spin-orbit component of the force necessary to explain the 6^- , $T=0$ cross section seems to vary significantly with energy from 300 to 800 MeV in a manner not explained by the Love-Franey force.

Analyzing powers were measured at 500 MeV from about 10° to 26° (q about 190 MeV/c to 485 MeV/c). The elastic-scattering A_y data from this experiment have appeared recently.¹¹ The present data are the first A_y data available above 200 MeV for these states which have been the subject of extensive cross-section measurements. Our theoretical analysis here uses the differential cross-section (σ) data of Ref. 10. The spin-rotation parameters D_{NN} , D_{LL} , D_{SS} , D_{LS} , and D_{SL} were measured at 17° and 22° (320 MeV/c and 415 MeV/c); no previous D_{ij} data on these states have been reported. The experiment is described in Sec. II and the results are presented in Sec. IV. The combinations D_K of these spin observables sensitive to particular components of the NN interaction have been formed, and all the data have been compared with RIA and NRIA theories. All calculations use free NN interactions to describe the inelastic transition, and inelastic form factors whose radii have been adjusted slightly relative to (e, e') form factors. Optical potentials were determined either from the NN interaction directly or from phenomenological fits to the elastic-scattering data. The theory is described in Sec. III; the calculations are presented in Sec. V. The results are discussed in Sec. VI.

II. EXPERIMENT

The data were taken at the High Resolution Spectrometer (HRS) at the Los Alamos Meson Physics Facility. The magnitude and direction of the incident beam polarization were monitored with a polarimeter based on scattering from a CH_2 target. For \hat{N} and \hat{S} polarization states, this was done continuously with a polarimeter in the beam line. For \hat{L} beams, the polarization was monitored from time to time with a polarimeter in an adjacent beam line where the rotation of the spin in the bending magnets yielded a transverse component. In all cases, the magnitude of the beam polarization was also monitored continuously by the quenching technique. The value of the beam polarization P_b was typically about 0.75, with variations of about ± 0.05 during the ten days of running. The absolute error in P_b is about ± 0.02 . The polarization of the scattered protons was measured by a polarimeter in the focal plane (FPP) of the HRS. This has been described previously.¹² By detecting the scattering from a block of graphite 13 cm thick with a set of large drift chambers, the azimuthal distribution of the scattering is determined and effective left-right and up-down differences can be measured. The effective analyzing power of the focal plane polarimeter was taken from the energy-dependent fit to the inclusive $p + {}^{12}\text{C}$ A_y data obtained by McNaughton *et al.*¹³ using the technique of Ransome *et al.*¹⁴ The central ray in the HRS is bent by 150° ; at 500 MeV, the corresponding rotation of the spin direction for a scattered proton with \hat{N} - or \hat{L} -type polarization is 412° . Because the HRS is a vertical spectrometer, a central proton with \hat{S} polarization suffers no spin rotation in the dipoles of the HRS. With an \hat{S} -type beam, then, the parity-allowed observables D_{SS} and D_{SL} can be measured simultaneously. The parameter D_{NN} is measured with an \hat{N} -type beam, and D_{LL} and D_{LS} are measured simultaneously with an \hat{L} -type beam. The ${}^{28}\text{Si}$ tar-

get was 50 mg/cm² thick. Beam quality during the run was comparatively poor and tuning parameters fluctuated with time. The primary effect was on the energy resolution which varied from about 60 to 100 keV during the run. A portion of the spectrum at 22° showing the two 6^- states at 11.58 MeV and 14.35 MeV is shown in Fig. 1; the resolution is about 75 keV. The two peaks stand out nicely here (and, of course, the 5^- is much cleaner since its cross section is about an order of magnitude larger), better than at other angles even though 22° is past the maximum of their angular distributions. There is little systematic error in extracting a value of A_y for each state by comparing two spectra like this for spin-up and spin-down beams. To extract a spin-rotation parameter, four spectra with many fewer counts must be compared (e.g., left and right scattering from the graphite with spin sideways left and spin sideways right). Small variations in the peak-fitting parameters can then lead to significant differences in the derived values of the observable, especially if the resolution is not as good as that shown here. A number of different methods of determining peak sums were tried with different methods of choosing "background." Reasonable variations in these methods generally yielded values of the observables within one standard deviation of the results shown below, where the errors shown are purely statistical. Other contributions to the systematic error in the D_{ij} for the 6^- states are small compared to peak-fitting errors. For the 5^- state, the systematic error is estimated at ± 0.04 .

III. THEORY

Microscopic calculations have been carried out in the framework of relativistic¹⁵ (RIA) and nonrelativistic impulse approximations (NRIA) for σ , A_y , and the D_{ij} . These are based on a nucleon-nucleon (NN) scattering amplitude of the (nonrelativistic) form:

$$M_\tau(q) = A_\tau + B_\tau \sigma_{1n} \sigma_{2n} + C_\tau (\sigma_{1n} + \sigma_{2n}) + E_\tau \sigma_{1q} \sigma_{2q} + F_\tau \sigma_{1p} \sigma_{2p} \quad (1)$$

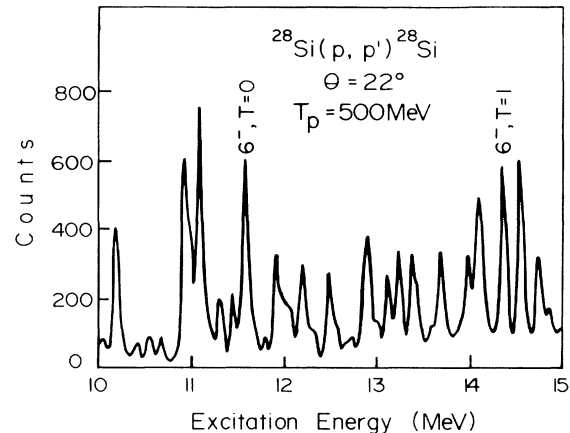


FIG. 1. Typical spectrum at high excitation energy for ${}^{28}\text{Si}(p, p')$ at $T_p = 500$ MeV and $\theta_L = 22^\circ$.

with $\sigma_{1n} = \sigma_1 \cdot \hat{\mathbf{n}}$, where $\hat{\mathbf{n}} = \mathbf{n}/|\mathbf{n}|$, etc. and $\mathbf{n} = \mathbf{k} \times \mathbf{k}'$, $\mathbf{q} = \mathbf{k}' - \mathbf{k}$, and $\mathbf{p} = \mathbf{q} \times \mathbf{n}$. Here \mathbf{k} and \mathbf{k}' are the initial and final proton momenta, and τ is the isospin index (0 or 1). The spin observables measured D_{ij} ($i, j = N, L, S$; N', L', S'), refer to directions defined in the *laboratory* helicity system where i refers to the incoming and j the outgoing spin components. $\hat{\mathbf{N}}$ is in the $\hat{\mathbf{n}}$ direction, $\hat{\mathbf{L}}$ in the \mathbf{k} direction, and $\hat{\mathbf{S}} = \hat{\mathbf{N}} \times \hat{\mathbf{L}}$. Similarly, $\hat{\mathbf{N}}' = \hat{\mathbf{N}}$, and $\hat{\mathbf{L}}', \hat{\mathbf{S}}'$ are defined relative to \mathbf{k}' . In the subsequent text we omit the prime on the second (outgoing) subscript.

As Bleszynski *et al.*⁴ and Moss⁵ have shown, certain combinations (D_K) of the D_{ij} are sensitive primarily to individual terms in the NN interaction. The D_K are given in terms of the D_{ij} as follows:

$$\begin{aligned} D_0 &= \frac{1}{4}[1 + (D_{SS} + D_{LL})\cos\theta_L + D_{NN} - (D_{LS} - D_{SL})\sin\theta_L], \\ D_x &= \frac{1}{4}[1 + D_{SS} - D_{LL} - D_{NN}], \\ D_y &= \frac{1}{4}[1 - (D_{SS} + D_{LL})\cos\theta_L + D_{NN} + (D_{LS} - D_{SL})\sin\theta_L], \\ D_z &= \frac{1}{4}[1 - D_{SS} - D_{NN} + D_{LL}], \end{aligned}$$

and

$$D_0 + D_x + D_y + D_z = 1, \quad 0 \leq D_K \leq 1. \quad (2)$$

In the plane-wave impulse approximation (PWIA) these quantities are, for unnatural parity states,

$$\begin{aligned} D_0^\tau &= \frac{|X_\tau^T|^2 |C_\tau|^2}{I_\tau}, \quad D_x^\tau = \frac{|X_\tau^L|^2 |E_\tau|^2}{I_\tau}, \\ D_y^\tau &= \frac{|X_\tau^T|^2 |B_\tau|^2}{I_\tau}, \quad D_z^\tau = \frac{|X_\tau^T|^2 |F_\tau|^2}{I_\tau}, \end{aligned} \quad (3)$$

where

$$I_\tau = |X_\tau^T|^2 (|C_\tau|^2 + |B_\tau|^2 + |F_\tau|^2) + 2|X_\tau^L|^2 |E_\tau|^2 \quad (4)$$

is the unpolarized cross section, and X_τ^T and X_τ^L are the transverse and longitudinal form factors defined as reduced matrix elements of the axial transverse electric and axial longitudinal multipole operators:¹⁶

$$X_\tau^T = \langle I^\pi, T \| \hat{\mathbf{T}}_e^5 \| 0^+, 0 \rangle, \quad (5)$$

$$X_\tau^L = \langle I^\pi, T \| \hat{\mathbf{L}}^5 \| 0^+, 0 \rangle. \quad (6)$$

For natural parity states in the PWIA,

$$\begin{aligned} D_0^\tau &= \frac{|Y_\tau^C|^2 |A_\tau|^2 + \frac{1}{2}|Y_\tau^M|^2 |C_\tau|^2}{I_0}, \quad D_x^\tau = 0, \\ D_y^\tau &= \frac{|X_\tau^C|^2 |C_\tau|^2 + \frac{1}{2}|Y_\tau^M|^2 |B_\tau|^2}{I_0}, \quad D_z^\tau = \frac{|Y_\tau^M|^2 |F_\tau|^2}{2I_0}, \end{aligned} \quad (7)$$

where

$$I_0 = |Y_\tau^C|^2 (|A_\tau|^2 + |C_\tau|^2) + \frac{|Y_\tau^M|^2}{2} (|B_\tau|^2 + |C_\tau|^2 + |F_\tau|^2) \quad (8)$$

is the unpolarized cross section, and Y_τ^C and Y_τ^M are the Coulomb transverse magnetic form factors defined as re-

duced matrix elements of the Coulomb and axial transverse magnetic multipole operators¹⁶

$$\begin{aligned} Y_\tau^C &= \langle I^\pi, T \| \hat{\mathbf{M}} \| 0^+, 0 \rangle, \\ Y_\tau^M &= \langle I^\pi, T \| \hat{\mathbf{T}}_{\text{mag}}^5 \| 0^+, 0 \rangle. \end{aligned} \quad (9)$$

When distortions are included, the D_K are still sensitive primarily to the same terms. Thus for the 5^- , $T=0$ state (populated mainly by A_0 and C_0 terms) we expect D_x and $D_z = 0$ and the ratio of D_y to D_0 is essentially a measure of the ratio of the spin-orbit (C) term to the central spin-independent term (A). For the 6^- , $T=0$ state, dominated by the isoscalar spin-orbit term (C_0), we expect D_0 to be large and the other D_K to be small. For the 6^- , $T=1$ state, where, in the calculations, the tensor force gives the main contribution, we expect D_x , D_y , and D_z to be larger than D_0 . (The tensor force contributes to the B , E , and F terms of the NN amplitude; the spin-orbit force only to the C term. For a pure tensor force without exchange, $E = 2B = 2F$.)

In this (PWIA) approximation, the relative size of D_0 , D_y , and D_z for the unnatural parity states is a direct indication of the magnitude of the C , B , and F terms in the NN interaction since the same nuclear form factor (X^T) enters into each. For stretched states, the ratio $|X_\tau^L|^2 / |X_\tau^T|^2$ is $2J/J+1$, so that D_x is also directly comparable.

Some qualitative indications about the values of the D_{ij} can be obtained from plane-wave considerations. For natural parity collective states, the rules for elastic scattering should be approximately obeyed:⁶ $D_{NN} \approx 1$, $D_{LL} \approx D_{SS}$, and $D_{LS} \approx -D_{SL}$. For unnatural parity states, Moss⁵ and Love and Klein¹⁷ have derived expressions which are simple if only one or two terms in the NN amplitudes contribute. For the $T=0$ state, dominated by C , all three diagonal D_{ij} should be roughly equal, large, and positive. For the $T=1$ state, the tensor force involves three amplitudes. If $B = F$, and C is neglected, then D_{NN} and D_{LL} should be roughly equal, large, and negative; D_{SS} depends sensitively on the ratio of B to E .

IV. EXPERIMENTAL RESULTS

The measured values of the A_y and the D_{ij} , along with previously reported¹⁰ values of σ , for the 5^- state are shown in Figs. 2–5. The curves in these figures are the results of theoretical calculations described below. Corresponding data for the 6^- , $T=0$ state are shown in Figs. 6–9, and those for the 6^- , $T=1$ state in Figs. 10–13. The error bars on the A_y data include a systematic error estimated at ± 0.015 . The D_{ij} data include statistical uncertainties only as discussed above; note that the error bars on these data at 22° are much smaller than at 17° .

The data for the 5^- state are similar to those reported previously for ^{40}Ca ,^{6,18,19} with a maximum value of $A_y \approx 0.6$ for both. The magnitudes of the D_{ij} are approximately equal to those for ^{40}Ca at the same qR . As in ^{40}Ca , the symmetry rules for elastic scattering are approximately followed, i.e., $D_{NN} \approx 1$, $D_{LL} \approx D_{SS}$, and $D_{LS} \approx -D_{SL}$.

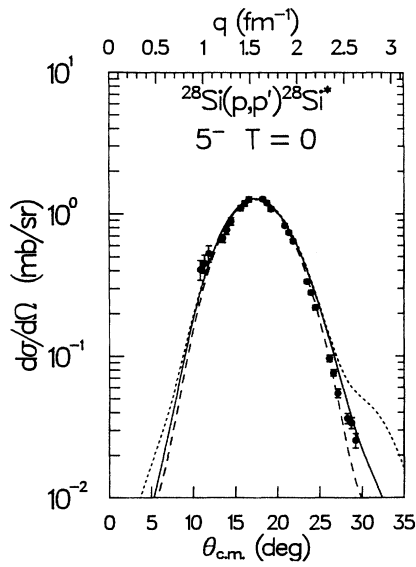


FIG. 2. Inelastic cross section for $^{28}\text{Si}(p,p')$ to the 5^- (9.70 MeV), $T=1$ state at $T_p=498$ MeV. The short-dashed curve is the RIA prediction. The NRIA-FOP prediction is shown as the long-dashed curve, and the NRIA-POP prediction as the solid curve. The data are from Ref. 10.

There are no previous A_y or D_{ij} data for unnatural parity states at large q at 500 MeV. At 180 MeV the measured A_y for the two 6^- states²⁰ are roughly similar to those observed here. The only D_{ij} data for high spin states are those reported by Olmer⁹ for the 4^- states in ^{16}O at 200 MeV; D_{NN} was not measured. For pure stretched states of high spin, the values of D_{ij} should be approximately independent of the nucleus, but not, of course, independent of energy unless the NN values are independent of energy. At the same q values as reported

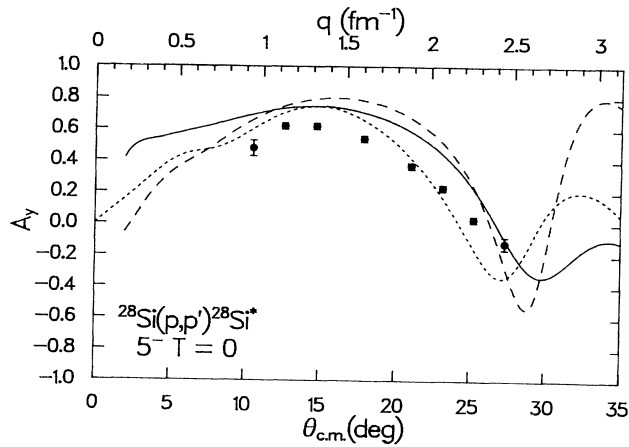


FIG. 3. Analyzing power for the 5^- (9.70 MeV) state in $^{28}\text{Si}(p,p')$ at $T_p=500$ MeV. The curves are described in the caption for Fig. 2.

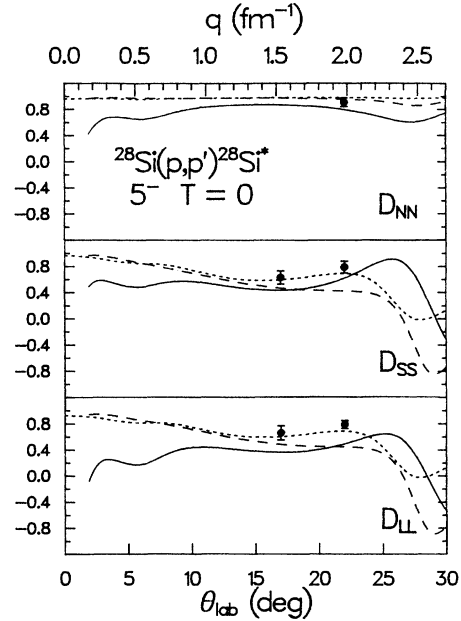


FIG. 4. Spin observables, D_{NN} , D_{SS} , and D_{LL} for $^{28}\text{Si}(p,p')$ to the 5^- (9.70 MeV) state at $T_p=500$ MeV. The curves are described in the caption for Fig. 2.

here, $D_{LL} \approx D_{SS} \approx 0.6-0.7$ for the two 4^- , $T=0$ states, very similar to our values. While the D_{SS} values for the $T=1$ states are roughly the same as D_{SS} for the 6^- , $T=1$ state here, the values of D_{LL} at 200 MeV tend to be more negative than at 500 MeV.

For the 6^- , $T=0$ state here, $D_{LL} \approx D_{SS} \approx D_{NN}$, in agreement with the PWIA predictions discussed above. Also, $D_{LS} \approx -D_{SL}$; differences here would be traceable to nonlocality effects expected to be much smaller than the errors here. For the 6^- , $T=1$ state, D_{NN} and D_{LL} are not equal, in contrast to the PWIA prediction, and both are far from the large negative values expected. In fact,

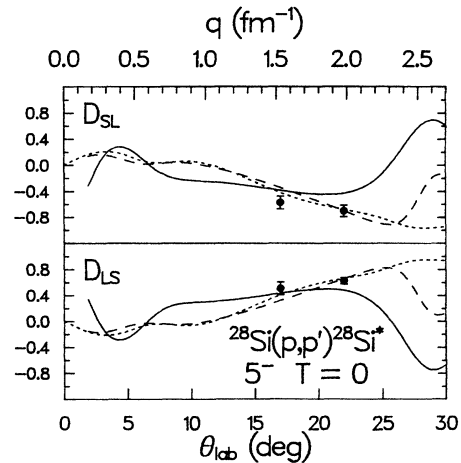


FIG. 5. Same as Fig. 4 but the observables are D_{SL} and D_{LS} .

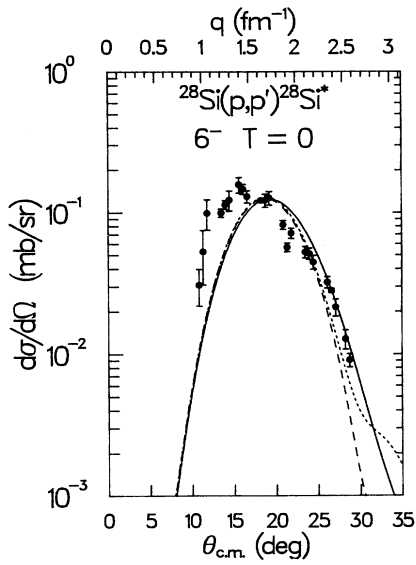


FIG. 6. Inelastic cross section for $^{28}\text{Si}(p,p')$ to the 6^- (11.58 MeV), $T=0$ state at $T_p=498$ MeV. The short-dashed curve is the RIA prediction. The NRIA-FOP prediction is shown as the long-dashed curve, and the NRIA-POP prediction as the solid curve. The data are from Ref. 10.

D_{SS} and D_{LL} are in closer agreement than D_{NN} and D_{LL} . Again, $D_{LS} \approx -D_{SL}$.

The values of the D_K formed from the D_{ij} are given in Table I for $\theta_L=22^\circ$ (D_{NN} was not measured at 17°). For the 5^- state, D_x and D_z are very close to zero as expected, and D_0 is dominant for the 6^- , $T=0$ state. But we also note that the value of D_0 for the 6^- , $T=1$ state is large, larger even than D_x and D_z . Like the D_{NN} and D_{LL} values discussed above, these values are surprising for this state, since its excitation, as predicted in the DWIA using the free NN interaction, is almost exclusive-

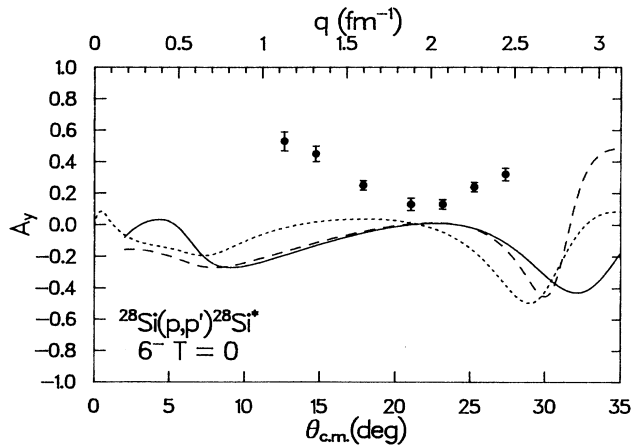


FIG. 7. Analyzing power for the 6^- (11.58 MeV), $T=0$ state in $^{28}\text{Si}(p,p')$ at $T_p=500$ MeV. The curves are described in the caption for Fig. 6.

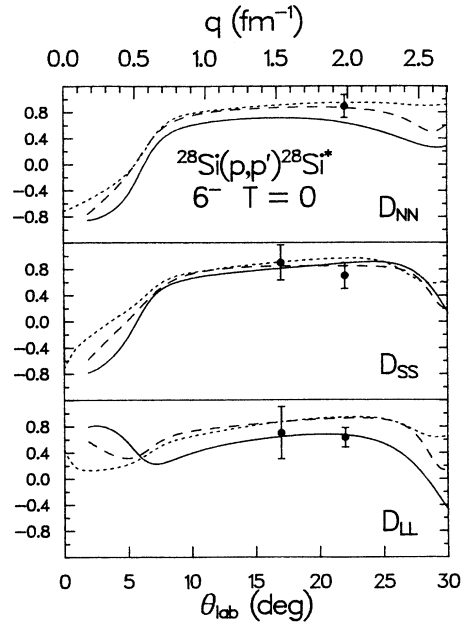


FIG. 8. Spin observables, D_{NN} , D_{SS} , and D_{LL} for $^{28}\text{Si}(p,p')$ to the 6^- (11.58 MeV), $T=0$ state at $T_p=500$ MeV. The curves are described in the caption for Fig. 6.

ly from the tensor interaction which contributes only to the B , E , and F terms in the NN amplitude [Eq. (1)]. These facts seem consistent with the need for a modification of the $T=1$ tensor force in medium, as suggested, for example, by theories indicating a reduction of the π and ρ meson masses in medium.²¹

V. CALCULATIONS

A. General

Microscopic calculations of σ , A_y , and the D_{ij} were carried out using both the RIA and NRIA for elastic

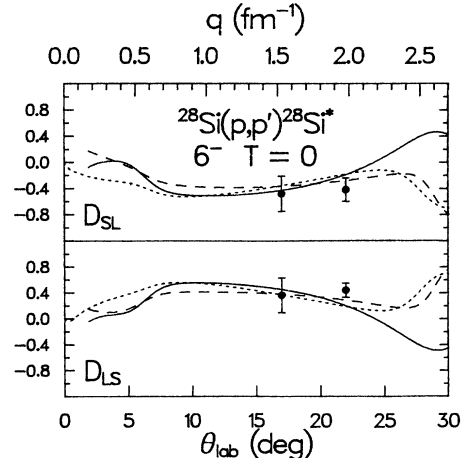


FIG. 9. Same as Fig. 8 but the observables are D_{SL} and D_{LS} .

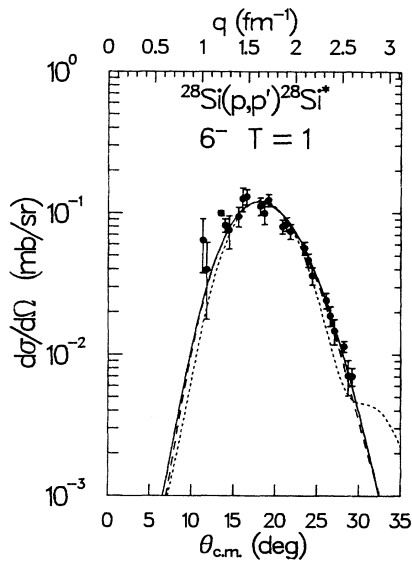


FIG. 10. Inelastic cross section for $^{28}\text{Si}(p,p')$ to the 6^- (14.35 MeV), $T=1$ state at $T_p=498$ MeV. The short-dashed curve is the RIA prediction. The NRIA-FOP prediction is shown as the long-dashed curve, and the NRIA-POP prediction as the solid curve. The data are from Ref. 10.

scattering and inelastic excitation of the three states of interest. Inelastic electron-scattering form factors were used as a guide in determining transition densities, although small changes in bound state radii (relative to those giving the best fit to electron scattering) were necessary to obtain the best fits to the (p,p') data. In both the RIA and NRIA the distorting optical potentials were calculated consistently (“folded optical potential” or FOP) using ground-state densities derived from electron scattering and a NN interaction derived from free NN amplitudes. The same NN interactions were used in the inelastic calculations. Since the elastic differential cross

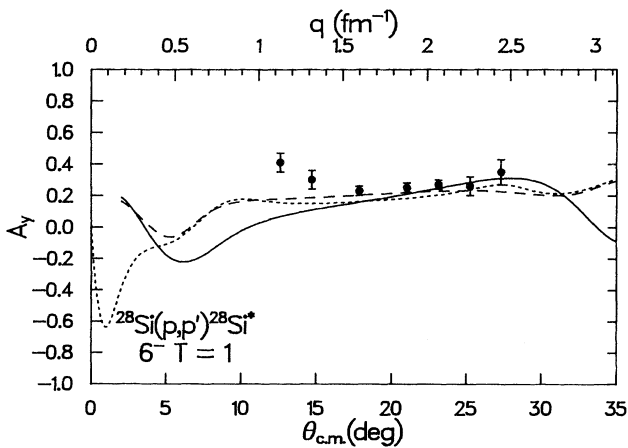


FIG. 11. Analyzing power for the 6^- (14.35 MeV), $T=1$ state in $^{28}\text{Si}(p,p')$ at $T_p=500$ MeV. The curves are described in the caption for Fig. 10.

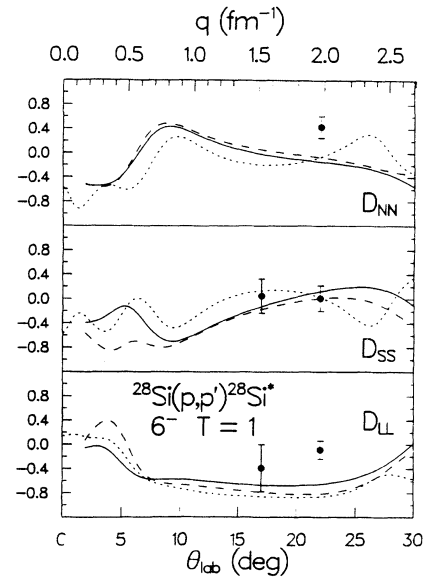


FIG. 12. Spin observables, D_{NN} , D_{SS} , and D_{LL} for $^{28}\text{Si}(p,p')$ to the 6^- (14.35 MeV), $T=1$ state, at $T_p=500$ MeV. The curves are described in the caption for Fig. 10.

sections predicted by the IA are less than perfect fits to the data, calculations were also made in the NRIA using a phenomenological optical potential (POP), adjusted to fit the elastic cross section and analyzing power data. With the programs available to us, it was not possible to use phenomenological distorting potentials in the RIA.

The RIA program used was DRIA, which has been described in the literature.¹⁵ For the NRIA calculations, programs ALLWORLD²² and DWBA70²³ were used. Both the RIA and NRIA programs make use of the free (on-shell) NN amplitudes of Arndt and Roper.²⁴ In the RIA the NN amplitudes are expanded in terms of local relativ-

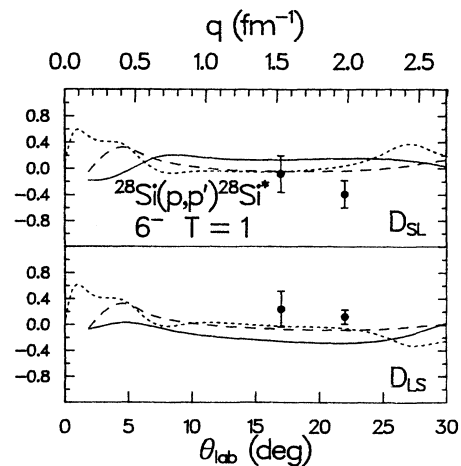


FIG. 13. Same as Fig. 12 but the observables are D_{SL} and D_{LS} .

TABLE I. D_K parameters at $\theta_L=22^\circ$ for $^{28}\text{Si}(p,p')$ at $T_p=500$ MeV.

State J^π, T		D_0	D_x	D_y	D_z	δD_K^a
$5^-, 0$	Expt.	0.72	0.02	0.24	0.023	± 0.03
	RIA	0.69	0.005	0.30	0.005	
	NRIA-FOP	0.56	0.006	0.42	0.016	
	NRIA-POP	0.62	0.085	0.27	0.02	
$6^-, 0$	Expt.	0.70	0.045	0.24	0.01	± 0.08
	RIA	0.89	0.018	0.082	0.008	
	NRIA-FOP	0.82	0.015	0.11	0.05	
	NRIA-POP	0.73	0.15	0.083	0.035	
$6^-, 1$	Expt.	0.29	0.17	0.42	0.12	± 0.08
	RIA	0.050	0.49	0.42	0.046	
	NRIA-FOP	0.049	0.47	0.41	0.064	
	NRIA-POP	0.132	0.48	0.30	0.092	

^aStatistical errors in D_K .

istic covariants and are parametrized in momentum space by a sum of Yukawa forms. In the NRIA programs, the Love-Franey⁸ coordinate space t matrix, also expressed as a sum of Yukawa potentials, was used. The phenomenological optical potential employed in the alternate NRIA calculation was obtained by a parameter search using the program RELOM.²⁵ These parameters are listed in Table II.

The electron-scattering calculations were made using programs ELECTL, ELECTE, ELECTM²⁶ (relativistic plane-wave Born approximations), and ALLWORLD²² (nonrelativistic plane-wave Born approximations). In the ELECT programs, contributions from the neutron charge form factor are not included so this was also omitted in the ALLWORLD runs. Both programs include the effects of the proton charge form factor. Omitting the neutron charge form factor decreased the peak value of $|F_L|^2$ (longitudinal form factor squared) by about 10% but left the shape unchanged, and it had no effect on F_T , the transverse form factor.

The cross-section data analyzed were from Refs. 27 and 28 (e, e'), and Ref. 10 (p, p'). The (p, p') A_y and D_{ij} data were from this experiment.

B. Electron scattering

For the $5^-, T=0$ states at 9.70 MeV the open-shell RPA amplitudes of Yen *et al.*²⁹ were used to construct the transition density. The state was assumed to be a

pure $T=0$ excitation. The bound-state wave functions were calculated in a Woods-Saxon potential with $a=0.65$ fm. The well depth was adjusted to give the binding energies listed in Table III. The reduced radius parameter r_0 was adjusted to give the best fit to the (e, e') total form factor. The values of r_0 and the resulting normalization parameters, $N_e^2 = (|F|_{\text{expt}}^2) / (|F|_{\text{theo}}^2)$ are listed in Table IV. It is seen that the nonrelativistic calculations require a bound-state radius $\sim 10\%$ larger than the relativistic ones, but give a similar normalization constant.

For the $6^-, T=1$ state at 14.35 MeV a single stretched configuration ($1d_{5/2}^{-1}, 1f_{7/2}$) was used in the calculation of the transition density. The bound-state radii and normalization factors are given in Table IV. Again it is seen that the nonrelativistic calculation requires a bound-state radius $\sim 10\%$ larger than the relativistic one for the best fit, but gives a similar normalization constant. No accurate (e, e') form factors are available for the $6^-, T=0$ state at 11.58 MeV. The calculated electron-scattering form factors are shown in Figs. 14–16.

C. Proton scattering

The same wave functions and bound-state parameters (except for r_0) as used for electron scattering were used in the proton calculations for the $5^-, T=0$ and $6^-, T=1$ states. In the nonrelativistic calculations a fixed spin-orbit term ($V_{\text{so}}=6$ MeV) was included in the bound-state potential. For most of the proton calculations (except in the RIA for the $6^-, T=1$ state) the bound-state potential radii needed to fit the data were slightly smaller than those which gave the best (e, e') fit as can be seen in Table IV. This need for an effective “shrinking” of the transition densities obtained from electron scattering has been seen previously for both elastic³⁰ and inelastic¹⁰ impulse-approximation proton scattering calculations. One effect which can produce this “shrinking” is a density-dependent modification of the NN t matrix due to a decrease of nucleon and meson masses inside nuclei as discussed in Refs. 30 and 31. Since, in this paper, we are interested in comparing predictions for proton spin observables in the RIA and NRIA, we have used transition densities which best fit the (p, p') cross-section data. The data for the $6^-, T=0$ state are somewhat less reliable than for the other two states due to the possible presence of neighboring unresolved states. Thus we have chosen a single value of the bound-state radius parameter for the three calculations.

The elastic distorted waves were calculated with a three parameter Fermi distribution for the ground-state charge density with $r_0=1.1$ fm, $a=0.58$ fm, and

TABLE II. Phenomenological optical potential (POP) (the potential is of the form: $U = Vf(r; r_v, a_v) + iWf(r; r_w, a_w) - (V_{LS} + iW_{LS})(\hbar/m_\pi c)^2(2/r)(d/dr)f(r; r_{LS}, a_{LS})\mathbf{l} \cdot \boldsymbol{\sigma} + V_C$ where V_C is the Coulomb potential of a uniformly charged sphere, $f(r; r_x, a_x) = [1 + \exp(r - R_x)/a_x]^{-1}$, and $R_x = r_x A^{1/3}$) parameters for $p + ^{28}\text{Si}$ at $T_p=500$ MeV (lengths in fm, energies in MeV).

r_c	V	r_v	a_v	W	r_w	a_w	V_{LS}	W_{LS}	r_{LS}	a_{LS}
1.05	-0.557	1.573	0.397	-24.5	1.203	0.550	-1.65	4.18	0.981	0.641

TABLE III. Single-particle energies used for bound-state wave functions (MeV).

State	5^-	$6^-, T=0$	$6^-, T=1$
$1d_{5/2}$	-17.2	-17.2	-17.2
$1d_{3/2}$	-5		
$1f_{7/2}$	-4	-2 ^a	-2
$1f_{5/2}$	-3		

^aNo significant difference was found between -2 and -4 MeV for the $1f_{7/2}$ energy.

$w = -0.233$.³² Proton and neutron charge form factors were unfolded to obtain the point proton density. The neutron density was assumed to be the same. The calculated elastic cross sections and analyzing powers are shown in Figs. 17 and 18. Both the RIA and NRIA (FOP) predictions have the same diffraction phase problem as noted above and so give relatively poor fits to the data as compared to the phenomenological optical potential (POP). This phase problem shows up in both the cross section and analyzing power data, as expected.

The inelastic σ , A_y , and D_{ij} predictions are shown in Figs. 2–13. The bound-state parameters and the cross-section normalizing factors used are given in Tables III and IV. The D_{ij} are plotted in the laboratory helicity system, as measured. The NRIA program DWBA70 gives this output directly, but the RIA program DRIA gives the D_{ij} in the center-of-mass helicity system. A small rotation ($\sim 1^\circ$) is needed to convert these to laboratory helicity, but this correction is $\sim 2\%$ or less and so it was ig-

TABLE IV. Bound-state potential reduced radii (r_0) and normalization factors, $N^2 = \sigma_{\text{expt}}/\sigma_{\text{theo}}$ for states J^π, T .

Calculation	$5^-, 0$		$6^-, 0$		$6^-, 1$	
	r_0	N^2	r_0	N^2	r_0	N^2
(e, e')						
RPWBA ^a	1.375	1.06			1.15	0.31
NRPWBA ^b	1.50	1.11			1.275	0.33
(p, p')						
RIA ^c	1.31	1.23	1.375	0.12	1.15	0.25
NRIA-FOP ^d	1.32	1.25	1.375	0.17	1.20	0.33
NRIA-POP ^e	1.375	0.83	1.375	0.13	1.25	0.26

^aRelativistic plane-wave Born approximation (ELECT).

^bNonrelativistic plane-wave Born approximation (ALLWORLD).

^cRelativistic impulse approximation (DRIA).

^dNonrelativistic impulse-approximation folded (consistent) optical potential (ALLWORLD and DWBA-70).

^eNonrelativistic impulse-approximation, phenomenological optical potential (RELOM, DWBA-70).

nored in view of the larger data error bars. The calculated values of the D_K parameters are given in Table I.

VI. DISCUSSION

The primary physics goals of this work were to investigate whether spin observables for inelastic scattering provided a signature for relativistic effects and to look for evidence of medium corrections to the NN force in nuclei. Comparison of theory and experiment in Figs. 2–13 suggests no strong overall preference for either the RIA or one of the NRIA calculations. The differences between RIA and NRIA predictions are mostly small com-

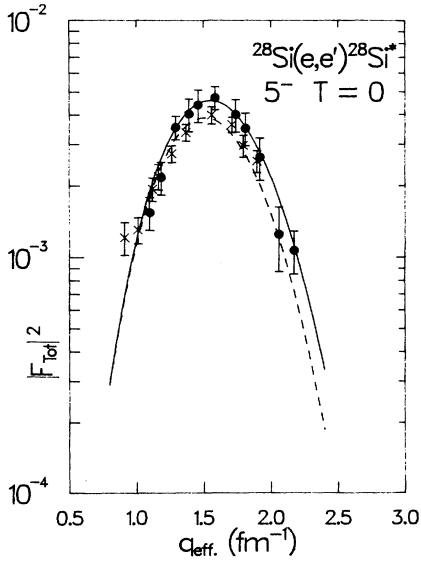


FIG. 14. Total form factor squared for $^{28}\text{Si}(e, e')$ to the 5^- (9.70 MeV), $T=0$ state at $\theta=90^\circ$ (crosses, dashed line) and $\theta=160^\circ$ (solid circles, solid line) vs q_{eff} . Curves are predictions of the relativistic plane-wave Born approximation. The data are from Refs. 27 and 28.

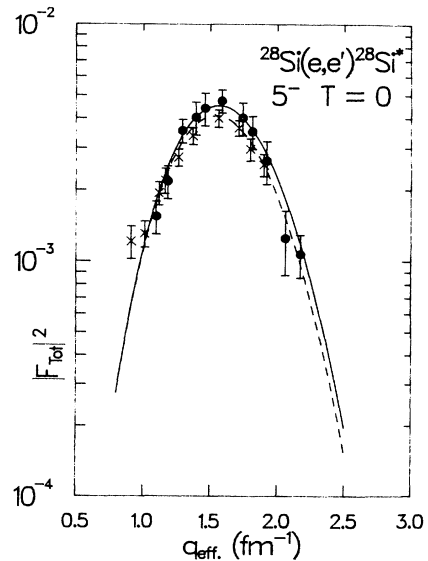


FIG. 15. Same as Fig. 14 but the curves are predictions of the nonrelativistic plane-wave Born approximation.

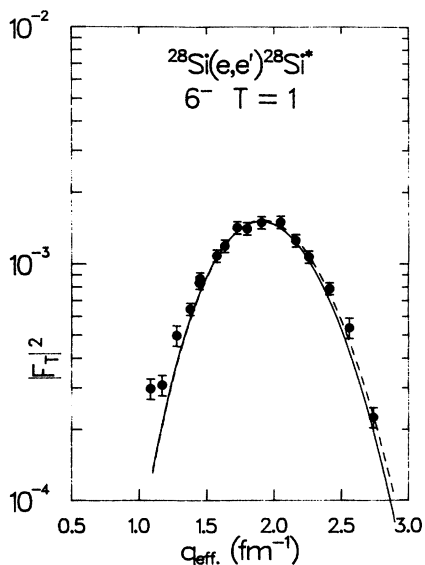


Fig. 16. Transverse form factor squared for $^{28}\text{Si}(e,e')$ to the 6^- (14.35 MeV), $T=1$ state. The solid curve is the prediction of the relativistic and the dashed curve the nonrelativistic plane-wave Born approximation. The data are from Refs. 27 and 28.

pared to the error bars on the data. When these differences are large, there is generally some preference for the RIA predictions. The most direct evidence of possible medium effects is the comparison of the theoretical and experimental values of the D_K in Table I. While the $T=0$ channel shows mostly excellent agreement be-

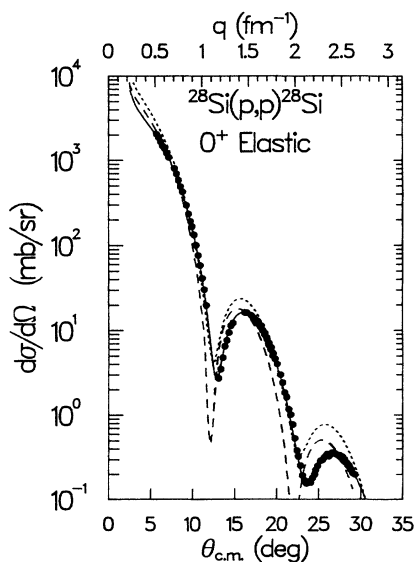


FIG. 17. Differential cross section for $p + ^{28}\text{Si}$ elastic scattering at $T_p = 498$ MeV. The short-dashed curve is the RIA prediction. The NRIA-FOP prediction is shown as the long-dashed curve, and the NRIA-POP prediction as the solid curve. The data are from Ref. 10.

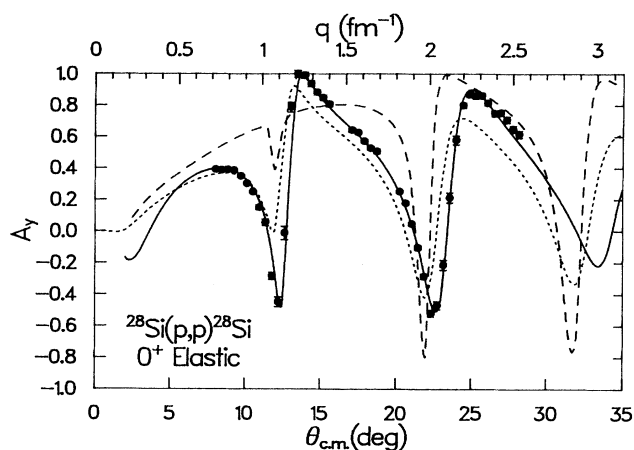


FIG. 18. Elastic analyzing power for $p + ^{28}\text{Si}$ at $T_p = 500$ MeV. The curves are described in the caption for Fig. 17.

tween the IA predictions and the D_K , the $T=1$ channel reveals several significant discrepancies.

For the 5^- state the RIA gives excellent agreement with the D_{ij} , although there is a small but significant deviation between the A_y data and theory. The NRIA fits (both FOP and POP) are significantly less good, especially for A_y , D_{SS} , and D_{LL} . The differences between the FOP and POP predictions are generally less than the deviations from the data. All four of the D_K parameters are in good accord with the RIA predictions, and they are reasonably close to the NRIA predictions as well.

For the 6^- , $T=0$ state, the predicted D_{ij} are in qualitative agreement with the data for both the RIA and NRIA calculations which differ little. The comparison between the experimental D_K (where the errors are smaller) and theory is also mostly good, though D_0 is slightly lower and D_y slightly higher than predicted. The predicted A_y , however, are in very poor agreement with the data; even the signs of the RIA and NRIA predictions are wrong. Since A_y is sensitive to interference between amplitudes, and the D_{ii} (but not the off-diagonal D_{ij}) only to the absolute square of amplitudes, the fact that serious problems appear only in A_y is not totally surprising.

For the 6^- , $T=1$ the predictions for A_y are fairly good; the NRIA is marginally better. The poor agreement with the D_{ij} could have been expected from the qualitative comments above based on plane-wave expectations. But the calculated values (in both the RIA and NRIA) do not satisfy these expectations very well either. While the predicted D_{LL} is large and negative the predicted D_{LL} does not equal D_{NN} and neither agrees with the data. For this state, only the predicted D_{SS} is within one standard deviation of the data. The differences between the qualitative expectations and the NRIA predictions were explored by comparing explicit PWIA calculations (with and without exchange) with the NRIA predictions shown. The PWIA predictions with a pure tensor force and the direct term only do indeed satisfy the qualitative expectations discussed. However, the distortions

have a significant effect on D_{NN} (but not on D_{SS} and D_{LL}), and the addition of exchange has a large effect on both D_{NN} and D_{SS} . The discrepancies between theory and experiment are mirrored in the problems with the D_K , where the predicted D_0 is much smaller and the D_x much larger than the data. These discrepancies may indicate a need for a reduction of the $T=1$ tensor force and an enhancement of the $T=1$ spin-orbit force in medium, as suggested by theoretical predictions based on the reduction of scalar and vector meson masses in medi-

um.^{21,30,31} Of course, a number of other possible mechanisms for changing the apparent NN force in nuclei remain to be explored as well. Confirmation of these results should be a high priority for future high-resolution studies of D_{ij} for stretched states in other nuclei over a range of incident energies.

This work was supported in part by grants from the U.S. National Science Foundation and Department of Energy and the Minnesota Supercomputer Institute.

*Present address: Lockheed Missiles and Space Co., Sunnyvale, CA 94089.

†Present address: CEBAF, Newport News, VA 23606.

¹B. C. Clark *et al.*, Phys. Rev. Lett. **50**, 1644 (1983); J. A. McNeil, J. R. Shepard, and S. J. Wallace, *ibid.* **50**, 1439 (1983); J. R. Shepard, J. A. McNeil, and S. J. Wallace, *ibid.* **50**, 1443 (1983).

²C. Glashauser *et al.*, Phys. Rev. Lett. **58**, 2404 (1987); F. T. Baker *et al.*, Phys. Lett. B **237**, 337 (1990).

³L. B. Rees, J. M. Moss, T. A. Carey, K. W. Jones, J. B. McClelland, N. Tanaka, A. D. Bacher, and H. Esbensen, Phys. Rev. C **34**, 627 (1986).

⁴M. Bleszynski, E. Bleszynski, and C. A. Whitten, Phys. Rev. C **26**, 2063 (1982).

⁵J. M. Moss, Phys. Rev. C **26**, 727 (1982).

⁶B. Aas, E. Bleszynski, M. Bleszynski, M. Haji-Saeid, G. Igo, F. Irom, G. Pauletta, A. Rahbar, A. T. M. Wang, J. F. Amann, T. A. Carey, W. D. Cornelius, J. B. McClelland, C. Glashauser, S. Nanda, M. Barlett, G. W. Hoffmann, and M. Gazzaly, Phys. Rev. C **26**, 1770 (1982).

⁷J. B. McClelland, J. M. Moss, B. Aas, A. Azizi, E. Bleszynski, M. Bleszynski, J. Geaga, G. Igo, A. Rahbar, J. B. Wagner, G. S. Weston, C. Whitten, Jr., K. Jones, S. Nanda, M. Gazzaly, and N. Hintz, Phys. Rev. Lett. **52**, 98 (1984); *ibid.* **52**, 954(E) (1984).

⁸M. A. Franey and W. G. Love, Phys. Rev. C **31**, 488 (1985).

⁹Catherine Olmer, *Antinucleon- and Nucleon-Nucleus Reactions* (Plenum, New York, 1985), p. 261.

¹⁰Norton M. Hintz, M. A. Franey, M. M. Gazzaly, D. Cook, G. S. Kyle, D. Dehnhard, S. J. Seestrom-Morris, G. W. Hoffmann, M. Barlett, G. S. Blanpied, J. A. McGill, J. B. McClelland, R. L. Boudrie, F. Irom, and G. Pauletta, Phys. Rev. C **30**, 1976 (1984); M. Gazzaly, private communication.

¹¹R. deSwinarski, D. Beatty, E. Donoghue, R. W. Ferguson, M. Franey, M. Gazzaly, C. Glashauser, N. Hintz, K. W. Jones, J. B. McClelland, S. Nanda, and M. Plum, Phys. Rev. C **42**, 1137 (1990).

¹²J. B. McClelland, J. F. Amann, W. D. Cornelius, H. A. Thiessen, B. Aas, and R. W. Ferguson, Los Alamos Report No. LA-UR-84-1671, 1984 (unpublished).

¹³M. W. McNaughton, B. E. Bonner, H. Ohnuma, O. B. Van Dyck, Sun Tsu-Hsun, C. L. Hollas, D. J. Cremans, K. H. McNaughton, P. J. Riley, R. F. Rodebaugh, Shen-wu Xu, S. E. Turpin, B. Aas, and G. S. Weston, Nucl. Instrum. Methods A **241**, 435 (1985).

¹⁴R. D. Ransome, C. L. Hollas, P. J. Riley, B. E. Bonner, W. D. Cornelius, O. B. Van Dyck, E. W. Hoffman, S. A. Wood, and

K. Toshioka, Nucl. Instrum. Methods **201**, 315 (1982).

¹⁵J. R. Shepard, E. Rost, and J. Piekarewicz, Phys. Rev. C **30**, 1604 (1984).

¹⁶T. W. Donnelly and W. C. Haxton, At. Data Nucl. Data Tables **23**, 103 (1979).

¹⁷W. G. Love and A. Klein, J. Phys. Soc. Jpn. Suppl. **55**, 78 (1986).

¹⁸K. K. Seth, D. Barlow, A. Saha, R. Soundranayagam, S. Iversen, M. Kaletka, M. Basko, D. Smith, G. W. Hoffman, M. L. Barlett, R. Ferguson, J. McGill, and E. C. Milner, Phys. Lett. **158B**, 23 (1985).

¹⁹B. Aas, E. Bleszynski, M. Bleszynski, M. Hajisaaid, G. J. Igo, F. Irom, G. Pauletta, A. Rahbar, A. T. M. Wang, J. F. Amann, T. A. Carey, W. D. Cornelius, J. B. McClelland, M. Bartlett, G. W. Hoffmann, and M. Gazzaly, Nucl. Phys. A **460**, 675 (1986).

²⁰G. T. Emery, A. D. Bacher, and C. Olmer, *Spin Excitations in Nuclei* (Plenum, New York, 1984), p. 371.

²¹G. E. Brown and M. Rho, Phys. Lett. B **237**, 3 (1990).

²²J. Carr, F. Petrovich, and J. Kelly, computer program ALLWORLD (unpublished).

²³R. Schaeffer and J. Raynal, computer program DWBA70 (modified); J. Raynal, Nucl. Phys. A **97**, 572 (1967).

²⁴R. A. Arndt and D. Roper, VPI and SU Scattering Analysis Interactive Dial-in Program and Data Base (unpublished).

²⁵G. J. Pyle, computer program RAROMP, University of Minnesota, Informal Report C00-1265-64, 1964 (unpublished), modified for relativistic energies.

²⁶J. R. Shepard, E. Rost, and J. A. McNeil, Phys. Rev. C **33**, 634 (1986). See also J. R. Shepard, E. Rost, E. R. Siciliano, and J. A. McNeil, *ibid.* **29**, 2243 (1984).

²⁷S. Yen, R. Sobie, H. Zarek, B. O. Pich, T. E. Drake, C. F. Williamson, S. Kowalski, and C. P. Sargent, Phys. Lett. **93B**, 250 (1980).

²⁸S. Yen, R. J. Sobie, T. E. Drake, H. Zarek, C. F. Williamson, S. Kowalski, and C. P. Sargent, Phys. Rev. C **27**, 1939 (1983); S. Yen, private communication.

²⁹S. Yen, R. J. Sobie, T. E. Drake, A. D. Bacher, G. T. Emery, W. P. Jones, D. W. Miller, C. Olmer, and P. Schwandt, Phys. Lett. **105B**, 421 (1981).

³⁰G. E. Brown, A. Sethi, and N. M. Hintz, Phys. Rev. C (to be published).

³¹G. E. Brown, C. B. Dover, P. B. Siegel, and W. Weise, Phys. Rev. Lett. **60**, 2723 (1988).

³²H. de Vries, C. W. de Jager, and C. de Vries, At. Data Nucl. Data Tables **36**, 495 (1987).